**THERMAL STABILITY OF FROZEN VOLATILES IN THE NORTH POLAR REGION OF MERCURY.**

David A. Paige[1], Matthew A. Siegler[1], John K. Harmon[2], David E. Smith[3], Maria T. Zuber[4], Gregory A. Neumann[3], Sean C. Solomon[5]. [1]Department of Earth and Space Sciences, UCLA, Los Angeles, CA 90095 (dap@moon.ucla.edu), [2]NAIC, Arecibo, PR 00612, [3]NASA GSFC, Greenbelt, MD 20771, [4]MIT, Cambridge, MA 02139, [5]Carnegie Institution of Washington, Washington DC, 20015.

**Introduction:** Earth-based radar observations have revealed the presence on Mercury of anomalously bright, depolarizing features that appear to be localized in the permanently shadowed regions of high-latitude impact craters [1]. Observations of similar radar signatures over a range of radar wavelengths implies that they correspond to deposits that are highly transparent at radar wavelengths and extend to depths of several meters below the surface [1]. Thermal models using idealized crater topographic profiles have predicted the thermal stability of surface and subsurface water ice at these same latitudes [2].

One of the major goals of the MESSENGER mission is to characterize the nature of radar-bright craters and presumed associated frozen volatile deposits at the poles of Mercury through complementary orbital observations by a suite of instruments [3]. Here we report on an examination of the thermal stability of water ice and other frozen volatiles in the north polar region of Mercury using topographic profiles obtained by the Mercury Laser Altimeter (MLA) instrument [4] in conjunction with a three-dimensional ray-tracing thermal model previously used to study the thermal environment of polar craters on the Moon [5].

**Methodology:** MESSENGER MLA data obtained poleward of 55° N were used to create a north polar digital elevation model (DEM) with a spatial resolution of 1 km [6,7]. So far, due to the inclination of the MESSENGER orbit, the highest density MLA coverage has been obtained in a circle surrounding the pole near 83°N, with lower density coverage at lower latitudes. The MLA DEM is the principal input for a three-dimensional ray-tracing thermal model that has successfully reproduced surface temperature observations in the south polar region of the Moon made by the Lunar Reconnaissance Orbiter (LRO) Diviner Radiometer Experiment [5]. The model has been modified to account for the average thermophysical properties and solar reflectance of Mercury's regolith, as well as Mercury's orbital and axial elements. For each point on a DEM, the model computes time histories of direct solar and multiply scattered solar radiation, emitted multiply scattered infrared radiation, and surface and subsurface temperature.

**Results:** Figures 1-3 compare Arecibo radar images with the MLA topography and model-calculated annual average and maximum surface temperatures for the region 83-65°N, 30-90°E. The annual average temperatures are representative of the expected temperatures at depths greater than ~0.4 m, the depth of penetration of Mercury's annual temperature wave [2]. The results show excellent general agreement between the locations of regions mapped as radar-bright from Earth and the locations of regions with low model-calculated temperatures. Figure 4 shows histograms of annual average and annual maximum temperatures for all areas shown in Figures 1-3 and those areas in Figure 1 that are radar-bright. Annual average temperatures in the radar-bright regions have a distinct peak at 100 K, and annual maximum temperatures in the radar-bright regions have a broader peak at ~170 K. Figure 4 also shows the volatility temperatures of ammonia, water ice, sulfur, and aromatic hydrocarbons. These are the temperatures at which these volatiles would sublimate to a vacuum at a rate of 1 mm per billion years [9,10].

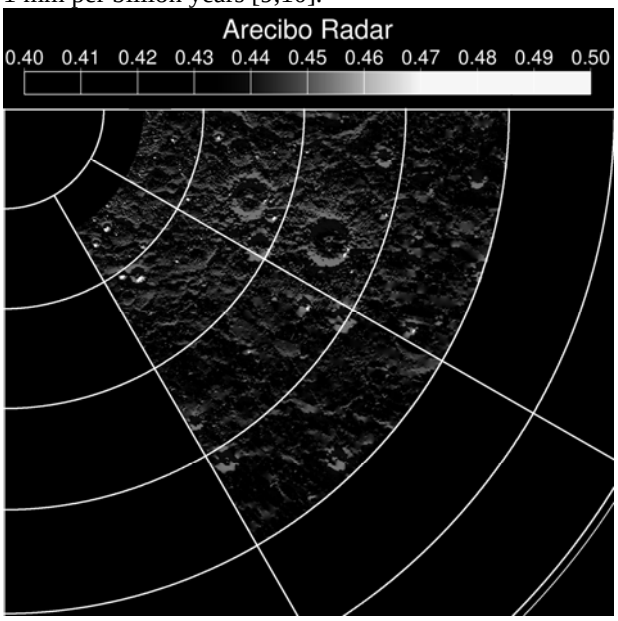


**Fig. 1.** Arecibo radar image of a portion of the north polar region of Mercury [8] superimposed on MLA topography [7].

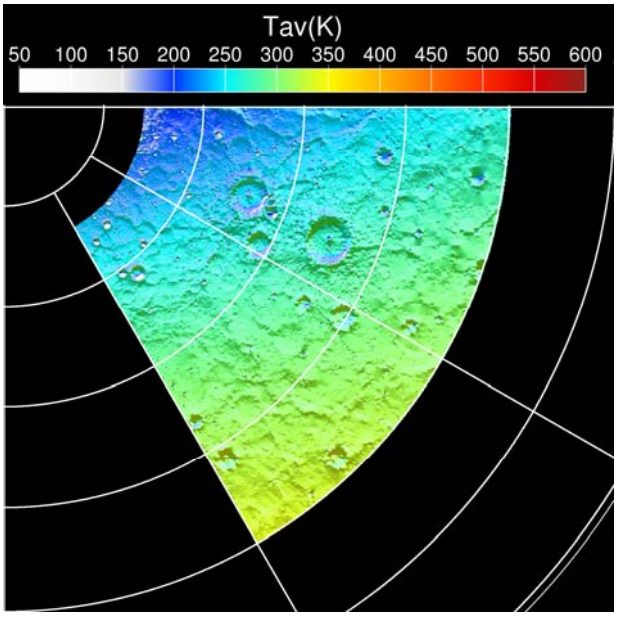


**Fig. 2.** Model-calculated annual average surface temperatures.

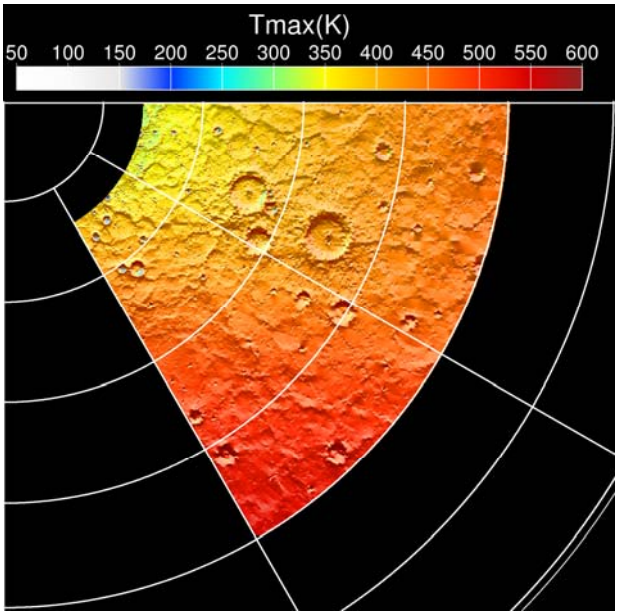


**Fig. 3.** Model-calculated annual maximum surface temperatures.

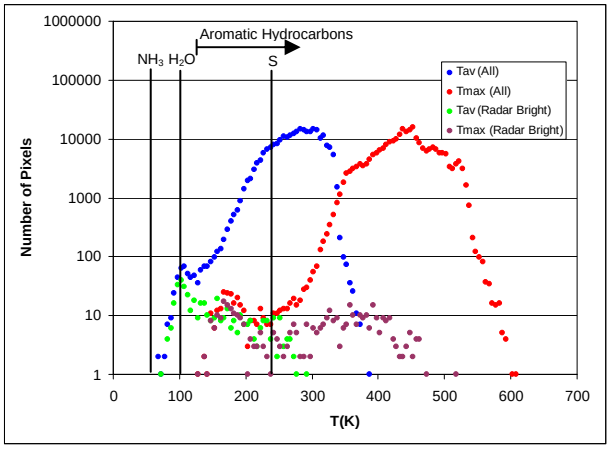


**Fig. 4.** Histograms of annual average and annual maximum surface temperatures for all the areas, and separately for the radar-bright areas, mapped in Figures 1-3. The volatility temperatures of ammonia, water ice, sulfur, and aromatic hydrocarbons are also indicated [9,10].

**Composition of Radar-Bright Features:** For the radar-bright regions shown in Figure 1, model-calculated annual maximum surface temperatures are too warm to permit the long-term thermal stability of exposed surface water ice deposits. In contract, approximately 10 cm below the surface, the thermal model calculations show that water ice should be thermally stable for billions of years. Less volatile aromatic hydrocarbons and sulfur may also be cold trapped at the surface and below the surface on Mercury. However, the fact that predicted subsurface temperatures in the radar-bright regions peak at the water ice volatility temperature is strong evidence that the radar-bright features mapped by MLA thus far are dominantly due to the accumulation of thermally stable subsurface water ice.

**Composition of Dark Surface Deposits:** In addition to mapping the topography of Mercury's north polar region, MLA observations are revealing that the reflectivities of radar-bright regions at 1064-nm-wavelength are distinctly lower than adjacent non radar-bright areas [7]. LRO Lyman-Alpha Mapping Project (LAMP) observations have detected analogous lower surface albedos at ultraviolet wavelengths in the permanently shadowed regions near the lunar north and south poles [11]. Both observations require that dark surface deposits are actively forming in regions of permanent shadow at rates faster than those for horizontal transport of regolith by impact gardening, which tends to spatially homogenize surface albedos. The LAMP team hypothesized that their lower observed albedos are due to a difference in regolith density [11]. The MLA results on Mercury and the thermal model results suggest that the lower albedos may instead be due to a difference in composition. Mercury is a very dark body, and there are few solar system materials that have lower albedos. The main exceptions are complex hydrocarbon compounds found in comets and volatile-rich asteroids [9,10] The results in Figure 4 show that surface temperatures in Mercury's radar-bright regions are in the correct range to actively cold-trap dark, impact-delivered hydrocarbon species. This leads us to suggest that the warmer near-surface regions of Mercury's polar cold traps may consist of a thin, ~10-cm-thick active layer of dark, organic-rich regolith that overlies thermally stable water ice [7].

**Comparison with the Moon:** Why do all the thermal niches for water ice on Mercury appear to be filled, whereas most of the Moon's niches appear not to be filled to nearly the same degree? Results from the Lunar Crater Observation and Sensing Satellite (LCROSS) experiments show that cold-trapped water and organics are definitely present on the Moon [12], but the ~35 K temperatures at the LCROSS impact site apparently prevent appreciable diffusive migration of water into the regolith [6]. On Mercury, temperatures are sufficiently warmer to permit much greater mobility of water. It is therefore likely that the process of impact deposition of volatiles and cold-trapping at the poles is occurring on both bodies, but the higher temperatures on Mercury have permitted water ice to become concentrated in polar cold traps to a much higher degree than on the Moon.

**References:** [1] Harmon, J. K. (2007) *Space Sci. Rev.* 132, 307. [2] Vasavada, A. R. et al. (1999). *Icarus* 41, 179. [3] Solomon, S. C. et al. (2001) *Planet. Space Sci.* 49, 1445. [4] Cavanaugh, J. F. et al. (2007) *Space Sci. Rev.* 131, 451. [5] Paige, D. A., et al. (2010) Science, 330, 479. [6] Zuber M. T. et al. (2012) Science, submitted. [7] Neumann, G. A. et al. (2012) *LPS* 43, this mtg. [8] Harmon, J. K. et al. (2010) Icarus 211, 37. [9] Zhang, J. A. and D. A. Paige (2009) *GRL* 36, L16203. [10] Zhang, J. A. and D. A. Paige (2010) *GRL* 37, L03203. [11] Gladstone, G. R. et al (2012) *JGR*, in press. [12] Colaprete, A. et al. (2010) *Science* 330, 463.